Effects of axial load on seismic performance of reinforced concrete walls with short shear span

by D.T.W. Looi[a], R.K.L. Su[a,*], B. Cheng[b], H.H. Tsang[c]

[a]*Department of Civil Engineering, The University of Hong Kong, Pokfulam Road, Hong Kong*

[b]*Beijing University of Civil Engineering and Architecture, Beijing, China*

[c]*Department of Civil and Construction Engineering, Swinburne University of Technology, Melbourne, Australia*

*Corresponding author. Email address: klsu@hku.hk (Ray K.L. Su).

ABSTRACT

Reinforced concrete (RC) shear walls in tall buildings are found to have a short shear span, particularly in high-degree coupled walls supported on transfer structures in low to moderate seismic regions. These non-seismically detailed walls in existing buildings are exposed to a high risk of failing in shear or compression before plastic hinges are formed at their base. Whilst previous research have focused on squat walls used in low-rise structures tested with zero or low axial loads, the structural response of these walls with a short shear span and limited ductility under high axial load is rarely discussed. Therefore, an experimental study that investigates the influence of the axial load ratio (ALR) on RC walls with a short shear span is presented in this paper. The specimens are designed with a low shear span-to-length ratio (SLR) and detailed with a characteristic 2% vertical and longitudinal reinforcement to represent a wall sub-structure above the transfer structure of tall buildings. Four walls are tested under reverse cyclic loading

and subjected to target ALRs that range from 0.1 to 0.4 to investigate the seismic performance until gravity collapse. The ALR is found to have significant effects on crack patterns, failure modes and deformability. Two modified empirical prediction models are proposed to estimate the shear strength capacity and ultimate drift ratio of rectangular RC shear walls with a short shear span under the effects of the ALR. A unique model of the drift limit of collapse under axial load as a function of the reinforcement ratio is put forward for performance based design and assessment.

Keywords: Reinforced concrete; Short shear span; Shear walls; Seismic behaviour; Axial load collapse

1. INTRODUCTION

1.1 Effects of short shear span on shear walls

Conventionally, shear walls were classified in accordance with their physical aspect ratio by using the height-to-length ratio (H/L), which led to the classification of walls as slender cantilever walls in many tall buildings. On the contrary, shear span, which is defined as the storey moment over storey shear ratio ($a = M/V$) as a result of internal stress response to lateral loads, is an alternate definition rather than simply referring to the physical height. The shear span of walls is greatly dependent on the height of the wall, pattern of the loading (a concentrated load or uniformly distributed load) and degree of coupling. A controlled cantilever wall that only allows flexural bending and only shows bending deformation is rare. Reinforced concrete (RC) buildings are either structurally framed with coupled shear walls or designed through the interaction between the wall and frame (dual structures), thus resulting in a certain degree of

reverse bending. In regions of low-to-moderately seismicity, highly over-strength coupling beams without strength hierarchy consideration are often used to optimise lateral elastic deflection of coupled shear walls under wind load. The low storey moment and high value of shear resulted in the formation of walls with a short shear span. Such effects are more critical for walls above transfer structures, which are concurrently under gravity and concentration of shear stress from lateral load due to the out-of-plane deformation of the transfer structures [1-2]. Hence, this special class of RC shear wall which has the distinctive features of short shear span and non-strength hierarchy design, is essentially a sub-structure at the base of a shear wall. These non-seismically detailed walls that have limited deformability in existing buildings have a high risk of failing in shear or compression before forming plastic hinges at their base in the event of an earthquake.

Fig. 1 shows a histogram of the shear span-to-length ratio (SLR) of the walls in a 45-storey tall RC building with transfer plates that support 40 storeys. The model was analysed by using ETABS, an engineering software [3]. It was found that the combination of high gravity load (average building density of 5.5 kN/m^3 in Hong Kong) and high wind load results in walls with an SLR that is less than 1.5. The definition of short shear span walls is illustrated in Fig. 1(c).

1.2 Effects of high axial load on shear walls

Post-earthquake investigations conducted after the 2010 M_w 8.8 Chile earthquake [4-5] showed that many shear wall buildings were seriously damaged. High axial load ratios (ALR = $P/f_{c,m}'A_g$, where P is the working axial load, $f_{c,m}'$ is the strength of the concrete cylinder and A_g is the gross cross section of the wall) were found to be the primary factor responsible for triggering the brittle failure of shear walls [4]. However, contrary to much of the research work on squat walls used in low-rise structures tested with zero or low axial load [6-8], and high axial load on slender walls

[9-11], the structural response of these walls with a short shear span and limited deformability under high axial load with gravity is rarely discussed.

Walls with such a low SLR are commonly treated as force-controlled components in capacity designs to ensure that the structure remains essentially elastic under maximum considered earthquake (MCE) ground motions that are typical in regions of moderate seismicity. However, in the rare event where the actual level of ground shaking exceeds the MCE level, allowing damage to the walls subject to a larger seismic displacement but ensuring that they do not lose their vertical load carrying capacity is challenging as noted in the current literature on shear walls. More importantly, the ALR was found to increase on average 50% when earthquake loads are added to the gravity load [11]. Therefore, this paper presents an experimental study that examines the influence of the ALR on rectangular shear walls with a short shear span, which are largely found in current building stocks in regions of low-to-moderate seismicity where vertical irregularities (such as transfer structures) are allowed in construction practices.

1.3 ALR limit of shear walls in design codes

A quick survey of the ALR limit in design codes around the world compared to the local design guide in Hong Kong shows that there is no consensus among the codes. The previous Structural Use of Concrete Code [12] in Hong Kong which followed the British Standards neither imposed limits on the ALR nor provided any seismic details. Thus, the ALRs of shear walls in many existing tall buildings are relatively high. In the 1997 Uniform Building Code [13], wall axial loads were limited to 0.35 P_0, where P_0 is the nominal axial load strength at zero eccentricity. Unfortunately, this limit is not correlated with the concrete strength, but merely based on an assumed corresponding balance point from a force-moment interaction diagram for wall piers. The American Concrete Institute (ACI) 318-14 [14] suggests that confinement is required where

the maximum extreme fibre compressive stress exceeds a critical value of 0.2 f_c'. The axial load corresponds to load combinations that include earthquakes. There is no limit in Standards New Zealand (NZS) 3101 [15] and its earthquake code NZS 1170.5 [16]; however, a wall with an ALR of 0.2 is considered to have a high axial load as stated in cl. 11.3.7. Yuen and Kuang [17] provided the ALR limits in Eurocode 8 [18], the most recent Structural Use of Concrete code of practice in Hong Kong [19] and the Chinese code GB50011 [20]. Their results seem to echo NZS 3101 [15], which recognises that a shear wall with an ALR greater than 0.2 is under a high axial load (and less than 0.2 is moderate). Hence, the experimental investigation will be conducted based on target ALRs of 0.1, 0.2, 0.3 and 0.4.

In the opinion of the authors, it is more convenient to standardise the vertical working load under gravity without bending due to lateral force (assumed as ultimate P_{ult} = 1.45 x working P) and the concrete is taken as the mean cylinder strength $f_{c,m}'$ (assumed as cylinder strength f_c' = 0.8 cube strength f_{cu}; and mean $f_{c,m}'$ = 1.5 characteristic $f_{c,k}$'). The following discussion will use this definition unless otherwise stated.

2. EXPERIMENTAL PROGRAMME

This experiment is based on a prototype of a typical tall RC building on a transfer structure located in Hong Kong (Fig. 1). The building is not seismically designed but subject to rather high wind load due to typhoons and hence the walls are strongly coupled with coupling beams to control roof drift. An SLR histogram showed that the majority of the walls above the transfer structure have an SLR that is less than 1.5. The sub-structure of the walls with a short shear span was scaled down to 1:4 to fit into the laboratory testing frame.

2.1 Details of wall specimens

Four RC wall specimens, which are labelled as C30-N-ALR01, C30-N-ALR02, C30-N-ALR03 and C30-N-ALR04, were fabricated and tested under different target ALRs (0.1 to 0.4). The dimensions of the walls were 800 mm in height x 800 mm in length x 80 mm in thickness; thus the aspect ratio is unity and the slenderness ratio is 1:10 (Fig. 2). The lateral load was applied at 950 mm above the concrete base (Fig. 3), which provided an SLR of 1.2. The concrete cover was taken as 20 mm at the side and 10 mm at the out-of-plane surface. Dimensions of the top beam of 400 mm in height x 900 mm in length x 180 mm in thickness, and bottom base of 400 mm in height x 1250 mm in length x 500 mm in thickness were designed to obtain a rigid component with properly anchored reinforcement from the walls. All of the walls were reinforced with high tensile ribbed (T10) vertical reinforcement bars that are 10 mm in diameter with 2% reinforcement and no boundary elements, and 1.4% plain (R8) horizontal stirrups that are 8 mm in diameter. Since the vertical reinforcement ratio is equal or greater than 2%, plain (R6) transverse tie bars that are 6 mm in diameter were included as per the Hong Kong Structural Use of Concrete Code [19]. The dimensions and reinforcement arrangement of the test specimens are shown in Fig. 2.

Table 1 shows the test matrix, which classifies the four specimens in accordance with the concrete strength, type of detailing and ALR, where the first three characters represent the target compression cylinder strength of the concrete, N denotes normal detailing, and the two numbers after the hyphen is the targeted ALR. For example, C30-N-ALR01 has a target concrete strength of 30 MPa and normal detailing with a target ALR of 0.1.

2.2 Materials

All of the concrete used to cast the specimens was mixed and cast-in-place in the concrete technology laboratory at the University of Hong Kong. The concrete strength f_c' was specifically set at 30 MPa in order to achieve the desired ALR under the limitations of the testing facility. The concrete had a maximum aggregate size of 10 mm and was mixed with ordinary Portland cement, sand (as fine aggregate), and water in addition to high-range water-reducing admixtures to improve the workability owing to the dense reinforcement configuration. Six cubes with dimensions of 150 x 150 x 150 mm and two standard cylinders that are 150 mm in diameter and 300 mm in height were also cast during the placing of the concrete to serve as the controls for the concrete strength evaluation. All of the concrete was covered with plastic and left to cure. All of the vertical reinforcements were fabricated with a nominal characteristic yield strength $f_{y,k}$ = 500 MPa, while all of the stirrups and transverse bars were fabricated with $f_{y,k}$ = 250 MPa. The reinforcements were purchased from a single local steel supplier. The measured strength of the concrete cylinders on the day of the wall test is given in Table 2, and the steel properties are shown in Table 3, where f_t is the tensile strength of the concrete obtained from indirect tensile testing by cylinder splitting, E_c is the modulus of elasticity of the concrete, A_s is the cross sectional area of the reinforcement, f_u is the ultimate tensile strength of the reinforcement and E_s is the modulus of elasticity of the reinforcement.

2.3 Experimental setup

The wall specimens with a short shear span were tested in a self-straining test rig with a diagonal strut on one side and supported by a strong floor (Fig. 3). Two vertical servo-controlled actuators that are capable of imposing a load of 500 kN with +/-150 mm were placed 600 mm apart from each other to produce the required ALR. In view of the effect from a high ALR and shear dominant deformation, the lateral drift was small and hence the P-delta effects and lateral

frictional force due to the vertical angle are negligible. A horizontal servo-controlled actuator that is capable of imposing a load of 500 kN with +/-250 mm was mounted onto a rigid transfer beam connected to the main columns with friction-bolted brackets to produce reverse cyclic loading. Two pairs of tailored one-sided push-pull rollers mounted on an out-of-plane support frame that was connected to the rigid RC top beam of the specimens via T-brackets bolted into cast-in anchors, were used to prevent out-of-plane deformation and buckling in the planar testing. The specimens were treated with high strength grout that was packed in between the soffit of the rigid RC base and the rigid platform to ensure that the base pressure was evenly distributed. Two sets of shoulder mounting devices were post-tensioned with eight high tensile M10.9 rods with a diameter of 20 mm to prevent uplift due to moment under cyclic loading. Stiffeners were placed on the rigid platform to act as stoppers to avoid lateral sliding of the specimens.

2.4 Instrumentation

The walls were instrumented with three distinct methods as shown in Fig. 4. On the front face, digital image correlation (DIC) was used to capture the full deformation field. Random black speckles were sprayed onto the walls with the use of a stencil board. The surface of the wall was coated with a thin layer of white plaster to enhance the contrasting. The random speckles were calibrated in accordance with diameter size: 1, 2.5, 5 and 10 mm. A Canon EOS 70D DSLR camera with a 20.2 megapixel sensor and Canon EF-S 18-55 mm IS STM lens captured the images of the random speckles in RAW format at 6-10 s intervals throughout the experiment. The ISO was set at 400 with an aperture of f/4. The camera was set in front of the test rig at about 2 m away from the walls with the focal length of the camera lens set at 24 mm, thus allowing about 2 pixels per mm ratio. In general, the speckles should be at a minimum 3-8 pixels in size to achieve effective correlation.

Point displacement measurement was carried out by using 23 linear voltage displacement transducers (LVDTs) at the side and rear of the walls, with reference to the rigid RC base of the walls to automatically eliminate unwanted base sliding between the specimen and the rigid platform (the frame that supports the LVDT stand is not shown in Fig. 4). LVDT 1 which was placed 950 mm above the RC base primarily controlled the drift displacement of the target in each cycle. Other measurements included those of the horizontal profile (with LVDTs 2 to 7), and vertical (LVDTs 8 to 12), diagonal (LVDTs 13 to 14), uplift (LVDTs 15 and16), sliding (LVDT 17) and out-of-plane (LVDTs 18 to 23) displacements. During the construction of the walls, 24 strain gauges were installed onto the vertical steel reinforcement (V1f-V16f and V1r-V16r) at the edges and 12 strain gauges (H1f-H6f and H1r-H6r) at the stirrups, where ‘f’ denotes the front and ‘r’ denotes the rear.

2.5 Loading protocol

On the day of testing, the concrete strength was first tested to determine the required axial load based on the target ALR. The total axial load was divided into half to be imposed by the two vertical actuators which would be simultaneously loaded onto the rigid RC top beam through displacement control. It is not possible to maintain a constant axial force in a displacement controlled protocol. Therefore, adjusting the gravity load during testing is necessary to circumvent the issue. The axial load was set at a range with a tolerance of +/-20 kN for each actuator, thus serving as the upper and lower bound values (Table 1). The two vertical actuators were controlled to move in the opposite displacement direction while at the same time subjected to reverse cyclic loading in the horizontal direction based on two repeated cycles at the drift ratio (DR) shown in Fig. 5. It is worth noting that the common loading protocol (with force based factor before yielding and ductility based factor after yielding) does not appear to be a good fit

with these wall specimens that have a limited ductility with a short shear span and therefore should not be used. The optimal velocity ratio of the vertical actuators to the horizontal actuators was about 1:6. All three actuators would stop if any of the vertical actuators approached the boundary value, and the axial load was accordingly adjusted. The benefit of displacement control is obvious in terms of safety precautions, but also allows more insights to be obtained through instrumentation data logging and DIC on the post-peak behaviour of walls with a short shear span. The tests were stopped when the specimens experienced an abrupt reduction in the axial force in the vertical direction and showed extremely low resistance to axial load thereafter in further drifts, which typically happens after shear failures.

3. ANALYSIS OF TEST RESULTS AND DISCUSSION

3.1 Observations on damage and failure mode

This study adopts DIC as a technique and no cracks were drawn manually at the peak of the drift cycles during the tests. Images acquired in RAW format during the tests were calibrated for camera type and lens distortion by using a DIC software, Optecal [21], for processing. Fig. 6 shows the plot of the failure crack patterns. Fig. 6(a) shows the DIC results of the front view of the wall with a short shear span at failure. Fig. 6(b) shows the DIC results of the front view when the walls are drifting in the opposite direction after experiencing failure, and Fig. 6(c) are the manually drawn cracks at the rear side of the wall after the LVDTs were removed. Significant concrete spalling which led to the disintegration of the concrete core was detected under a low ALR but this was reduced when subjected to a high ALR. Horizontal flexural cracks were first detected at the side boundary of the walls, which initiated from the base of the wall. They

occurred at the stirrup location along the height of the wall. The direction of these horizontal cracks then rotated and joined the diagonal shear cracks at the web of the walls. Large diagonal cracks (approximately 0.3 mm in width) that propagated from corner to corner were observed on the wall specimen under low axial load (i.e., C30-N-ALR01). The cracks became hairline in width when the ALR was increased (i.e., C30-N-ALR04), and the direction of the crack propagation turned inward towards the centre of the base.

The observed phenomenon of a rotated crack propagation can be physically explained with a strut-and-tie model. There were wider cracks on the C30-N-ALR01 specimen which failed due to the failure of the diagonal strut, where the edge longitudinal reinforcements were found yielded in tension, causing a cyclic tension-compression load excursion. The failure of the C30-N-ALR03 and C30-N-ALR04 specimens was due to shear-compression as a result of the failure of the fan shaped strut, which induced significant crushing of the web at their base. The crushing of the web was a brittle failure and accompanied by a loud noise. The C30-N-ALR02 specimen had a mixed failure mode due to compression failure of both the diagonal strut and the fan shaped strut. The fan shape strut was balanced off by the elastic tension of the edge longitudinal reinforcements, causing a cyclic compression-compression load excursion, and hence the crack angle was rotated due to the significant compression zone at the edge which did not induce yielded tensile strains. These observed shear compression failures agree well with those in Paulay et al. [22], but are more insightful because axial load variations are also incorporated.

An important observation of the out-of-plane instability (buckling) due to in-plane loading [23] was also made after the crushing of the web. Fig. 7 shows two distinct types of out-of-plane buckling of the two extreme bounds of the ALR values, in which a peculiar phenomenon can be observed at the original centreline (by laser light) and the centreline of the wall thickness. At a

very low ALR (C30-N-ALR01 specimen), there is evidently local reinforcement buckling at the edge of the wall at maximum drift, yet this does not lead to axial failure. The axial load is redistributed to the remaining vertical bars with 2% reinforcement. At the other extreme with a high ALR, global buckling of the reinforcement with an obvious buckling length was detected after the removal of the concrete specimen (C30-N-ALR04 specimen in Fig. 7(b)). Since the test was conducted under displacement-controlled axial loading, there was no disastrous pancake type of collapse after the buckling of the reinforcements, but instead, a significant reduction in vertical displacement was found in LVDTs 8 and 9.

Interestingly, premature shear sliding was not observed, which contrasts the situation of many squat walls discussed in the literature [22, 24]. This is likely due to the application of axial stress which increases the compression zone of the base of the wall, which does not allow the reinforcements to easily yield in tension (in the case of C30-N-ALR02 to ALR04). For the C30-N-ALR01 specimen, the heavily reinforced vertical reinforcements which did not yield in flexural tension, provided sufficient dowel action even though a significant portion of the concrete had spalled. Evidence of insignificant shear sliding is demonstrated by the non-pinched hysteresis curve discussed in the next section.

3.2 Load deflection hysteresis curve

The pre-peak, post-peak to ultimate shear and axial collapse of the wall specimens with a short shear span are shown in the load deflection hysteresis curve in Fig. 8. All of the yield information of the reinforcements was obtained from the installed strain gauges. The hysteresis curves change from a full to a narrow loop with an increase in the ALR, thus indicating that high axial loads reduce the energy dissipation capacity. The maximum shear strength of all the specimens is almost identical, recorded at approximately 250 kN, due to the sufficiently

reinforced 1.4% R8 stirrups tested at a yield of 289 MPa which added up to about 250 kN. All of the stirrups were not found yielded in the wall specimens. The vertical T10 steel bars with 2% reinforcement provided a large amount of reinforcement which allowed the C30 concrete to resist shear. Hence, no increase of the shear strength was observed under the effects of the ALR. This phenomenon can be explained by using the compression field theory with Mohr's circle. However, the deformability of the walls was suppressed as a higher axial load was applied. This can be seen in the very limited DR of C30-N-ALR03 (0.63%) and C30-N-ALR04 (0.47%), where an ultimate DR is assumed to be the commonly recognised shear failure, a point where the wall experiences a 20% reduction of peak shear. The application of a moderate ALR for C30-N-ALR02 means that a DR of about 1% can be attained. The peak shear and ultimate drift values are listed in Table 4.

The behaviour of C30-N-ALR01 is consistent with many commonly reported wall failures in the literature [25], where tension yielding (vertical rebar at the edges), concrete spalling, shear failure and residual shear strength are present in the hysteresis model (Fig. 8). The vertical reinforcements in the wall can withstand vertical loading, in which no loss of axial capacity was observed after losing its shear capacity. This failure mode was often reported to be desirable, but realistically the ALR in the wall specimens with a short shear span is greater than 0.2. Very often in cases where there is a higher ALR (the C30-N-ALR02, C30-N-ALR03 and C30-N-ALR04 specimens), the vertical reinforcements yield during compression and buckle, accompanied by crushing of the concrete web. For higher ALRs, axial collapse takes place almost right after shear failure, and there is no residual shear strength which is contrary to the experimental evidence in the C30-N-ALR01 specimen and contradicts with the recommendation in Table 10-20 of ASCE41 [26]. Even though the ALR can be controlled if it is low which appears to be a

quick exit in design practices, extreme concrete spalling which causes the concrete core to disintegrate may require special attention. In such a scenario (ALR $\leq$ 0.1), the load path for gravity systems should be protected.

3.3 Degradation of lateral secant stiffness

Fig. 9 shows the variations in the secant stiffness in the first cycle for each DR. Specimens with a higher ALR show a higher initial secant stiffness. That is, the secant stiffness of the C30-N-ALR04 and C30-N-ALR03 specimens is higher than that of the C30-N-ALR02 and C30-N-ALR01 specimens. The degradation of the lateral secant stiffness as determined from the slope of the initial DRs (<0.25%) did not seem to be influenced by the ALR. After the DR exceeds 0.25%, the secant stiffness continued to severely degrade for the cases with a high ALR (C30-N-ALR03 and C30-N-ALR04 specimens), and the degradation stopped at a lower DR of about 0.5%. Contrary to the cases with a high ALR, the slope of the degradation became gentler at a DR of 0.25% for the C30-N-ALR01 and C30-N-ALR02 specimens, thus suggesting that the ALR has a significant influence on degradation of lateral stiffness at a higher DR for cases with a lower ALR.

3.4 Degradation of axial stiffness

The lateral secant stiffness as discussed in the previous section has been commonly reported in the literature on wall tests; however, axial stiffness is a less discussed area. Fig. 10 illustrates the unique pattern variations of the axial stiffness of the wall specimens with a short shear span, which is taken at the top centre of the specimens with averaged forces from the vertical actuators and averaged displacements from LVDTs 8 and 9. Fluctuations in the axial stiffness can be observed in the C30-N-ALR01 and C30-N-ALR02 specimens. These wall specimens show axial

tensile extension at certain drifts due to the tension of the vertical reinforcements, rotation of the diagonal strut in the concrete, and unrecoverable cracks. Degradation of compression induced axial stiffness can be observed in the cases with a high ALR (the C30-N-ALR03 and C30-N-ALR04 specimens) from the previous fluctuating behaviour. Table 4 summarises the applied axial stress over the ultimate shear stress capacity (p/v where p is the applied axial stress and v is the ultimate shear stress capacity) of the walls. In the opinion of the authors, a p/v ratio of 2 seems to be the point that differentiates between the two different types of axial stiffness behaviour.

3.5 Out-of-plane deformation

Out-of-plane failure patterns have been frequently reported; for instance, in recent earthquakes in Chile and New Zealand [25,] and are observed physically in the testing in this study (Fig. 7). A more detailed picture of the out-of-plane deformation patterns is shown in Fig. 11, where LVDTs 22 and 23 which are located near the base of the walls are used as the reference. Considerable out-of-plane deformation can be observed in all of the wall specimens. For the C30-N-ALR01 specimen, the out-of-plane deformation developed without causing severe degradation to its global axial capacity as can be observed in its hysteresis curve, and lateral secant stiffness and axial stiffness behaviours. Nonetheless, the unrecoverable point of degradation is attributed to the local buckling of the vertical reinforcements at the boundary edge at a DR of +1.0%. For the rest of the wall specimens that have a higher ALR (the C30-N-ALR02, C30-N-ALR03 and C30-N-ALR04 specimens), an unrecoverable point of the out-of-plane deformation was found on each wall which corresponded to the direction and the DR of the axial failure. Out-of-plane deformation is an indicator of buckling instability caused by compression. A potential solution to

this problem could be well-detailed boundary elements that provide confinement, but this is beyond the scope of this paper.

3.6 Proposed ultimate shear capacity

In a previous study carried out by the authors of this study [27], a comprehensive database of 183 rectangular squat RC walls (with squat walls generally defined as SLR $\leq$ 2.5) was generated, in which the data were obtained from various experiments in the current literature from 1995 to 2016, to predict the maximum shear capacity with emphasis on the effects of axial load prior to conducting the experiments in this paper. The theoretical shear capacity ($V_f = M_f/a$, ratio of flexural moment to the shear span) of the wall specimens with a short shear span can be categorised into either shear (Zone S) or flexural (Zone F) failure mode by plotting a simple axial-moment interaction curve that compares the shear capacities obtained in the experiment (V_{exp}), which is a similar approach to the one that classifies RC columns in Zhu et al. [28]. A plus minus 10% band is imposed for ambiguous shear-flexural modes. In this paper, the results obtained from all of the wall specimens, some wall tests (with and without boundary elements) that were carried out in collaboration with the Beijing University of Civil Engineering and Architecture (BUCEA), and the latest wall tests from the literature are taken into consideration. In accordance with the histogram in Fig. 1, the SLR was further restricted to less than or equal to 1.5. Since the same database was used for prediction of shear and drift, only cyclically loaded walls were included, as it is known that using monotonic load can lead to overestimation of the drift capacity of walls. Further filter criteria were imposed onto the database to control the validity of the rectangular wall data. The criteria included: (i) no lap splices or couplers, (ii) no diagonal reinforcement, (iii) complete information of test results obtained until post peak failure, (iv) no composite materials, for instance, steel tubes embedded at boundary elements instead of

reinforcements, and (v) symmetrical boundary elements. Finally, the database information was categorised into 25 Zone S and 34 Zone F (shear-flexure bending) walls with a short shear span (Fig. 12) [29]. A statistical multi-parameter regression analysis was conducted to modify the predictive empirical models for seismic shear capacity. The proposed model in Eq. (1) predicts the normalised shear stress ratio (v/f_c') which is dimensionless, incorporates the shear span to effective depth ratio (a/d) as a parameter coupled with the ALR and various mechanical reinforcing ratios to form linear functions of coefficients A to D. Linear function charts are provided for design applications, see Fig. 13.

$$\frac{v}{f_c'} = 0.02 + A\,(ALR)^{0.4} + B\,\omega_v + C\,\omega_h + D\,\omega_{v,be} \le 0.5$$
$$\text{where} \quad A = 0.15 - 0.10\,a/d$$
$$B = 0.60 - 0.25\,a/d \qquad (1)$$
$$C = 0.80 - 0.20\,a/d$$
$$D = -0.08 + 0.10\,a/d$$

where ω_v, ω_h and $\omega_{v,be}$ are the mechanical ratio of the vertical longitudinal reinforcement, horizontal stirrups and vertical reinforcement of the boundary elements on one side, respectively and are defined in Equation (2).

$$\omega_v = \rho_v \frac{f_{yv}}{f_c'}; \quad \omega_h = \rho_h \frac{f_{yh}}{f_c'}; \quad \omega_{v,be} = \rho_{v,be} \frac{f_{y,be}}{f_{cc}'} \qquad (2)$$

where ρ_v is the vertical and longitudinal reinforcement ratio, ρ_h is the horizontal stirrup ratio, $\rho_{v,be}$ is the vertical reinforcement ratio of the boundary elements on one side, f_{yv} is the yield strength of the vertical longitudinal reinforcement, f_{yh} is the yield strength of the horizontal stirrups, $f_{y,be}$ is the yield strength of the vertical reinforcements at the boundary elements and f_{cc}' is the confined concrete strength of the boundary elements. It should be noted that the reinforcement ratios (ρ_v, ρ_h and $\rho_{v,be}$) are in decimal numbers (not percentage) when applying the model. The effective

shear depth (d) is assumed to be 0.8 L, which is consistent with the recommendations in ACI 318 Cl. 11.5.4.2 [14] and CSA A23.3 Cl. 21.5.9.2 [15].

The concrete strength, which is confined by hoops in the boundary elements, is taken into account by using the experimentally observed relationship in [30] and modified in Eq. (3).

$$f_{cc}' = f_c' + C_{conf}\ \rho_{hoopbe,vol}\ f_{yhoop}$$

where

$$C_{conf} = \min\left[1, \sqrt{\left(\frac{l_{be}}{s_{v,hoop}}\right)\left(\frac{l_{be}}{s_{h,vbe}}\right)\left(\frac{1}{\rho_{hoopbe,vol}\ \frac{f_{yhoop}}{f_c'}}\right)}\right] \quad (3)$$

where l_{be} is the length of the boundary elements along the in-plane direction of the wall specimen, $s_{v,hoop}$ is the vertical distance of the hoops in the boundary elements, $s_{h,vbe}$ is the horizontal distance of the vertical reinforcements in the boundary elements along the in-plane direction of the wall specimen, $\rho_{hoopbe,vol}$ is the volumetric ratio of the hoop steel reinforcements (in percentage) and f_{yhoop} is the yield strength of the hoops.

Eq. (1) implicitly considers the components that contribute to the shear strength of concrete (v_c), axial compression (v_p) and steel reinforcements (v_s), with a simple derivation that is shown below in Eq. (4).

General form:

$$\frac{v}{f_c'} = \text{constant} + A\,(ALR) + B\,\omega_v + C\,\omega_h + D\,\omega_{v,be}$$

Contributing components: (4)

$$v = \left[\text{constant}\, f_c'\right] + \left[A\,(ALR)\, f_c'\right] + \left[B\,\rho_v\, f_{yv} + C\,\rho_h\, f_{yh} + D\,\rho_{v,be}\, f_{ybe}\,\frac{f_c'}{f_{cc}'}\right]$$

$$v = v_c + v_p + v_s$$

By benchmarking the test results of the wall specimens with a short shear span as summarised in Table 4, the effects of the ALRs are obtained more effectively as compared to the previous predictions that are merely based on the collected information in the database with projected ALRs [27]. Fig. 14(a) shows the corroboration of the experimental results with the proposed ultimate shear capacity model of the wall specimens with a short shear span, with a near to unity mean and median, and minimum coefficient of variation (COV). The COV of 28.4% is considered acceptable in shear capacity study as demonstrated in Grammatikou et al. [31]. Table 4 shows the computed values of the shear strength of the walls tested in this study by using Eq. (1).3.7 Proposed ultimate drift capacity

Likewise, the prediction of the ultimate DR at shear failure (assumed to occur at a commonly recognised shear failure state that corresponds to 80% of the peak load) for Zone S walls with a short shear span as proposed in Looi et al. [32] is slightly modified specifically for SLRs ≤ 1.5 and presented in Eq. (5).

$$DR_{ult}(\%) = 0.85(50)^{\left(0.64\frac{v}{f_c'}\frac{a}{d}\right)} 0.1^{ALR}\, 0.6^{\omega_v}\, 2.6^{\omega_h}\, 1.3^{C_{conf}} \le 2.5 \quad (5)$$

where the normalised maximum shear stress ratio (v/f_c') can be estimated by using Eq. (1) and the other symbols in the equation have already been defined in the previous equations shown above. The corroborated results of predictions of the drift with those obtained by the experiments are shown in Fig. 14(b), which verifies the reliability of the model with an acceptable COV. It is noted that the prediction of the drift capacity is relatively more scattered than the shear capacity as demonstrated in Table 4 of Grammatikou et al. [31]. The computed ultimate DR values of the walls tested in this study with Eq. (5) are reported in Table 4.

3.8 Drift limit of collapse under axial load

Wallace et al. [33] examined the limit of drift of lightly reinforced wall piers under axial load based on a shear-friction model. This model which is capable of predicting the drift capacity of typical wall piers prior to the loss of vertical load bearing capacity is exceptionally useful for understanding and setting the drift performance criteria in performance based seismic design. To take into consideration the lightly reinforced wall piers which have damage due to diagonal shear friction, an empirical model for heavily reinforced walls with a short shear span ($1\% < \rho_v \leq 2\%$ and $1.0 \leq \text{SLR} \leq 1.5$) is proposed here for damage from shear compression buckling. Eq. (6) modifies the ALR into a more generic format so as to incorporate the effects of longitudinal reinforcements in an inelastic state.

$$ALR' = \frac{P}{\left[\rho_v f_{yv} + (1-\rho_v) f_{cm}'\right] A_g} \tag{6}$$

Fig. 15 depicts the relationship between the newly defined ALR′ and the DR (Eq. (7)), where the DRs at the onset of and immediately after axial failure recorded during the test are highlighted for reference. All symbols are consistent and defined previously in the text.

$$ALR' = 0.85 \exp\left[-1.8\, DR_{\text{collapse}}(\%)\right] \tag{7}$$

A boundary condition is implicitly specified in Eq. (7), where the ALR′ maximum is taken as 0.85, a factor commonly used for rectangular stress blocks in a compression zone. It is important to note that when the reinforcement itself in the compression strain zone (even with a disintegrated concrete core) is sufficient enough to resist low axial load (as in the case of the C30-N-ALR01 specimen), the drift limit under axial load can be considerably extended. The associated DRs of the axial collapse of the walls tested in this study with Eq. (7) are shown in

Table 4. The contribution of the boundary elements in ductile walls tested in collaboration with the BUCEA [29] were considered in the formulation of Eq. (7). A practical case study of two RC walls with a short shear span and with and without boundary elements is presented in the following section.

3.9 Case study of RC walls with a short shear span

To demonstrate the effects of the ALR for Eqs. (1), (5) and (7), a case study of three RC walls with a short shear span is shown in Fig. 16(a) along with their properties. The local mean value of the concrete and steel strength was based on Su et al. [34]. The boundary elements were varied with C_{conf} of 0.2 and 0.4 to simulate the level of confinement by varying the hoop spacing. Fig. 16(b) shows the variations in shear prediction under different ALRs. Ductile walls with a short shear span and detailed boundary elements can marginally increase the shear capacity as compared to a limited ductile wall with a short shear span. The shear capacity is observed to increase with the ALR; nonetheless, it is still highly dependent on the reinforcement ratio to mobilise the full shear strength of the concrete.

Fig. 16(c) illustrates the changes in the deformation limit in terms of the DR under different ALRs. The generic formulation of an ultimate DR at shear failure by using Eq. (5) shows the effectiveness of boundary elements (C_{conf} dependant) in enhancing the deformability of walls compared to the limited ductile walls with a short shear span. However, by overlaying the drift limit under axial load by using Eq. (7) onto the same graph, it is found that collapse under axial load is prevented and instead, there is a lower DR limit under higher ALRs, despite the use of detailed boundary elements. This observation is thus far valid under the condition of heavily reinforced walls with a short shear span ($1\% < \rho_v \leq 2\%$ and $1.0 \leq \text{SLR} \leq 1.5$).

3.10 Drift limit in performance based seismic design

An updated version of ASCE-41, which contains guidelines for performance based seismic design of buildings [26], differentiated the level of shear wall performance into: (i) walls controlled by flexure based on plastic hinge rotation (in Table 10-19), and (ii) walls controlled by shear based on the DR (in Table 10-20). The four walls in this study with a short shear span and controlled by shear are used to examine their performance level in terms of immediate occupancy (remains elastic after an earthquake, and buildings with these walls can be immediately occupied afterwards), life safety (extensive damage sustained by building after earthquake but walls remain stable, so that occupants can still access the building) and collapse prevention (building is still standing but has sustained substantial damage) per Table 10-20 in ASCE-41. The effects of the axial load were calculated with the information in Table 10-20, and all of the wall specimens were found to exceed 0.05. It is noted that the ASCE-41 requirement is stringent in terms of ALR limit but unconservative in terms of DR limit, hence new proposal is made here. Fig. 17 shows the DR of the four wall specimens in this study in terms of the performance level. For the case of short shear span RC walls, two categories are proposed in accordance to the ALR. For short shear span walls with ALR < 0.2 shown in Fig. 17(a), the immediate occupancy level is recommended as 0.4%, being the same as the recommendation in ASCE-41 [26]. Judging from the limit of the collapse of the C30-N-ALR02 specimen under axial load, which has an ALR of 0.22, it is proposed that the ALR limit in ASCE-41 [26] is modified from 0.15 to 0.2. The life safety level is proposed to fall in the range of 0.5% to 0.75% and DR > 0.75% is considered as the collapse limit.

Although categorising walls with a high ALR as force-controlled components for capacity design appears to be a common method in high seismic regions, allowing walls to undergo

damage subject to larger seismic displacement under the rare event of an earthquake in low-to-moderate seismic regions requires special attention. Hence, for walls with $0.2 \leq \text{ALR} \leq 0.4$, the immediate occupancy level is benchmarked at a DR of 0.25% in this study, in view of the almost undisturbed slope of the lateral secant stiffness as shown in Fig. 9 and the essentially elastic slope of the hysteresis curve in Fig. 8. Fig. 17(b) shows the performance levels suggested for cases with a higher ALR (C30-N-ALR03 and C30-N-ALR04 specimens), where 0.25% to 0.4% is the acceptable DR for life safety and collapse is anticipated after 0.5% in view of the limited DR of 0.47% of the C30-N-ALR04 specimen with an actual ALR = 0.44. It is further proposed that the ALR of walls should not be more than 0.4.

4. CONCLUSIONS AND RECOMMENDATIONS

Four RC walls with a short shear span, aspect ratio of 1.0, SLR of 1.2 and 2% vertical reinforcements are experimentally tested to failure under gravity collapse with target ALRs of approximately 0.1, 0.2, 0.3 and 0.4, respectively, to investigate the seismic performance of non-seismically detailed walls as a sub-structure supported on a transfer structure. This unique irregular vertical structural form is allowed in construction practices in many low-to-moderate seismic regions. The following conclusions are made based on the work in this study.

1. With increased ALRs, the failure mode of heavily reinforced walls with a short shear span changes from compression with a diagonal strut (wide diagonal cracks) to crushing of the web due to shear compression from a fan shaped strut (hairline diagonal cracks), which eventually leads to local and global buckling of the vertical reinforcement bars accompanied by crushing of the concrete at the compression zone near the base of the wall.

2. Out-of-plane instability due to in-plane loading is observed in all of the wall specimens. An unrecoverable point of out-of-plane deformation is detected in each wall specimen which corresponds to the direction and the DR of axial failure..
3. Higher ALRs prevent the deformability of walls with a short shear span. Even though controlling the ALR at a low level appears to be a quick solution in design practices, extreme concrete spalling which causes the concrete core to disintegrate may require special attention. In this scenario (ALR $\leq$ 0.1), the load path of the gravity systems should be protected .
4. An interesting observation of the variations in axial stiffness with ALR is identified, where the axial stress to shear stress capacity ratio (p/v) can be used to differentiate the failure mode with the diagonal strut to the failure due to shear compression with a fan shaped strut. A p/v ratio of less than 2 appears to be the point where the axial stiffness fluctuates and a ratio of more than 2 shows degradation of the axial stiffness (compression).
5. Two modified empirical prediction models are proposed to estimate the shear strength capacity and the ultimate DR of (SLR $\leq$ 1.5) rectangular RC wall specimens with a short shear span under the effects of ALR.
6. A unique DR limit of collapse under axial load that comprises a reinforcement ratio for heavily reinforced walls is proposed to complement a model on collapse of lightly reinforced wall piers due to shear-friction under axial load [32], to arrive at a more fitting ALR limit for performance based designs.
7. A practical case study of three RC walls with a short shear span with and without boundary elements is presented to demonstrate the use of the proposed equations in this study. It is found that collapse under axial load imposes a lower DR limit under higher ALRs compared to the ultimate DR in shear failure, despite the use of detailed boundary elements. This

observation is thus far valid under the condition of heavily reinforced walls with a short shear span ($1\% < \rho_v \leq 2\%$ and $1.0 \leq \text{SLR} \leq 1.5$).

8. The DR limit is proposed by reconciling with ASCE-41 [26]. Two categories of DR limits are proposed for performance based seismic design, where the first category is for wall with ALR < 0.2 and the second category is for wall with $0.2 \leq \text{ALR} \leq 0.4$. The value of the limits were highlighted in Fig. 17.
9. Shear and axial failures can simultaneously occur at relatively low drift levels under high ALRs. The minimum ultimate drift capacity associated with the shear and axial failures of walls with a short shear span is found to be as low as about 0.47% under an ALR of 0.4 in this study. This means that building occupants are given no warning before axial failure occurs. Engineers must be therefore able to identify shear walls that may experience this catastrophic failure mode, and focus more on the effects of the load path of gravity systems rather than only the lateral load resisting systems. A short term quick fix is to limit the ALR in structural framing or apply capacity design factors to encourage formation of flexural hinges. However, in the longer term, investigation of the seismic behaviour of walls with a short shear span under unavoidable high axial loads is essential for low-to-moderate seismic regions, particularly when there are vertical irregularities. For future research work, the recommendations are to: (i) address out-of-plane buckling failure with thicker webs and lower slenderness ratios, (ii) validate limits of collapse of shorter walls under axial load with $0.5 < \text{SLR} < 1.0$, (iii) test with a reinforcement ratio of 1%, and (iv) explore innovative ways to circumvent the issue of the limited ductility of walls with a short shear span under high ALRs.

ACKNOWLEDGEMENTS

The research carried out in this paper gratefully acknowledges financial support from the Research Grants Council of the Hong Kong SAR (Project No. HKU 17202315). The advice and help from the staff and students of the HKU Civil Engineering Laboratory who assisted with the tests presented in this paper are greatly appreciated.

REFERENCES

[1] Su RKL, Cheng MH. Earthquake induced shear concentration in shear walls above transfer structures. The Structural Design of Tall and Special Buildings 2009;18(6):657-671.

[2] Tang TO, Su RKL. Gravity-induced shear force in reinforced concrete walls above transfer structures. Proceedings of the Institution of Civil Engineers: Structures and Buildings 2015;168(1):40-55.

[3] CSI. ETABS integrated building design software introductory user's guide, Computers and Structures, Inc. Berkeley, California, USA; 2003.

[4] Westenenk B, de la Llera JC, Besa JJ, Junemann R, Moehle J, Luders C, Inaudi JA, Elwood KJ, Hwang SJ. Response of reinforced concrete buildings in Concepcion during the Maule Earthquake. Earthquake Spectra 2012;28(S1), S257-280.

[5] Carpenter LD, Naeim F, Lew M, Youssef NF, Rojas F, Saragoni GR, Adaros MS. Performance of tall buildings in Vina del Mar in the 27 February 2010 offshore Maule, Chile earthquake. The Structural Design of Tall and Special Buildings 2011;20:17-36.

[6] Hidalgo PA, Ledezma CA, Jordán RM. Seismic behavior of squat reinforced concrete shear walls. Earthquake Spectra 2002;18(2):187-208.

[7] Kuang JS, Ho YB Seismic behavior and ductility of squat reinforced concrete shear walls with nonseismic detailing. ACI Structural Journal 2008;105(2):225-231.

[8] Luna BN, Rivera JP, Whittaker AS. Seismic behavior of low-aspect-ratio reinforced concrete shear walls. ACI Structural Journal 2015;112(5):593-604.

[9] Zhang YF, Wang ZH. Seismic behavior of reinforced concrete shear walls subjected to high axial loading. ACI Structural Journal 2000;97(5):739-750.

[10] Su RKL, Wong SM. Seismic behaviour of slender reinforced concrete shear walls under high axial load ratio. Engineering Structures 2007;29(8):1957-1965.

[11] Alarcon C., Hube MA, de la Llera JC. Effect of axial loads in the seismic behavior of reinforced concrete walls with unconfined wall boundaries. Engineering Structures 2014;73:13-23.

[12] Buildings Department (BD). Code of Practice for Structural Use of Concrete 2004. The Government of the HKSAR, Hong Kong; 2004.

[13] Uniform Building Code (UBC). International Council of Building Code Officials. Whittier, CA; 1997.

[14] ACI Committee 318. Building Code Requirements for Structural Concrete (ACI 318M-14) and Commentary (ACI 318RM-14). Farmington Hills, MI: American Concrete Institute; 2015.

[15] NZS 3101:2006. Concrete structures standard, Part 1 – the design of concrete structures. Wellington: Standards Association of New Zealand; 2006.

[16] NZS 1170.5:2004. Structural Design Actions, Part 5 – Earthquake actions. Wellington: Standards Association of New Zealand; 2004.

[17] Yuen YP, Kuang JS. Effect of axial compression on ductility design of RC walls. Structures and Buildings 2015;168,554-569.

[18] BS EN 1998-1:2004. Eurocode 8: Design of structures for earthquake resistance. Part 1: General rules, seismic actions and rules for buildings. BSI, London, UK; 2004.

[19] Buildings Department (BD). Code of Practice for Structural Use of Concrete 2013. The Government of the HKSAR, Hong Kong; 2013.

[20] National Standard of People's Republic of China GB50011-2010. Code for seismic design of buildings. MCPRC (Ministry of Construction of the People's Republic of China), China Architecture & Building Press, Beijing, China; 2010.

[21] Optecal DIC Software, CV Measurements, Berkeley, CA; 2015.

[22] Paulay T, Priestley MJN, Synge AJ. Ductility in Earthquake Resisting Squat Shearwalls. ACI Journal 1982;79(4):257-269.

[23] Dashti F., Dhakal RP, Pampanin S. Development of out-of-plane instability in rectangular RC structural walls. 2015 New Zealand Society for Earthquake Engineering (NZSEE) Annual Technical Conference. 10-12th April. Rotorua, New Zealand; 2015.

[24] Schuler H, Trost B. Sliding shear resistance of squat walls under reverse loading: mechanical model and parametric study. ACI Structural Journal 2016;113(4):711-721.

[25] Sritharan S, Beyer K, Henry RS, Chai Y, Kowalsky M, Bull D. Understanding poor seismic performance of concrete walls and design implications. Earthquake Spectra 2014;30(1):307-334.

[26] ASCE/SEI 41-13. Seismic Evaluation and Retrofit of Existing Buildings. ASCE Standard. Reston, Virginia, US; 2014.

[27] Looi DTW, Su RKL. Predictive seismic shear capacity model of rectangular squat RC shear walls in flexural and shear zones. Proceedings of 16th World Conference on Earthquake Engineering, 16WCEE, Jan 09-13, Santiago, Chile; 2017.

[28] Zhu L, Elwood KJ, Haukaas T. Classification and seismic safety evaluation of existing reinforced concrete columns. ASCE Journal of Structural Engineering 2007;133(9):1316-1330.

[dataset] [29] Looi DTW. Filtered database of Short Shear Span RC Walls (M/VL <= 1.5), Researchgate.net data, v1; 2017. DOI: dx.doi.org/10.13140/RG.2.2.27730.15047.

[30] Saatcioglu M., Razvi SR. (1992): Strength and ductility of confined concrete. Journal of Structural Engineering, 118 (6), 1590-1607.

[31] Grammatikou S, Biskinis D, Fardis MN (2015): Strength, deformation capacity and failure modes of RC walls under cyclic loading. Bulletin of Earthquake Engineering, 13, 3277-3300.

[32] Looi DTW, Su RKL, Cheng B, Zhou MJ. Ultimate drift prediction models of rectangular squat reinforced concrete shear walls", in Hao & Zhang (Eds.), Mechanics of Structures and Materials: Advancements and Challenges; Taylor & Francis Group, London. 2017;1653-1659.

[33] Wallace JW, Elwood KJ, Massone LM. Investigation of the axial load capacity for lightly reinforced wall piers. Journal of Structural engineering 2008;134(9):1548-1557.

[34] Su RKL, Looi DTW, Tang TO, Law CW. Performance based seismic design for tall buildings in Hong Kong. Proceedings of presentation at HKIE/IStructE Joint Structural Division Annual Seminar 2014 Advances in Seismic Engineering, May 19, Jockey Club Auditorium, The Hong Kong Polytechnic University; 2014.

Tables and Figures

List of Tables:

List of Figures:

Fig. 8 – Load-displacement hysteresis curve

Fig. 9 – Degradation of lateral secant stiffness

Fig. 10 –Degradation of axial stiffness

Fig. 11 – Out-of-plane deformation due to in-plane loading

Fig. 12 – Filtered database of rectangular squat RC walls categorised into Zones S and F

Fig. 13 – Linear functions of proposed shear capacity model for Zone S

Fig. 14 – Corroboration of experimental results with (a) proposed ultimate shear capacity model for Zone S (b) proposed ultimate drift ratio model for Zone S

Fig. 15 – Limit of drift due to collapse under axial load for wall with short shear span

Fig. 16 – Case study - effects of ALR on wall with short shear span (a) properties of walls, (b) variation in shear capacity with ALR, (c) variation in drift ratio capacity with ALR

Fig. 17 – Proposal of the inter-storey drift that corresponds to various performance levels of wall specimens with reference to ASCE-41 [26] (a) walls with ALR < 0.2 (b) walls with $0.2 \leq ALR \leq 0.4$

Table 1 **– Test matrix of wall specimens with short shear span**

Specimen	Range of axial load, kN	Average axial load (P), kN	ALR
C30-N-ALR01	180 - 260	220	0.12
C30-N-ALR02	350 - 420	380	0.22
C30-N-ALR03	640 - 720	680	0.38
C30-N-ALR04	740 - 820	780	0.44

Table 2 – Concrete properties of tested specimens

Specimen	Concrete cylinder strength (f_c'), MPa	Concrete tensile strength (f_t), MPa	Modulus of elasticity of concrete (E_c), MPa
C30-N-ALR01	29.1	2.94	21397
C30-N-ALR02	26.4	3.04	21589
C30-N-ALR03	27.6	2.67	19805
C30-N-ALR04	28.0	2.30	18155

Table 3 – Properties of steel reinforcements of tested specimens

Type of steel reinforcement	Steel area (A_s), mm^2	Yield strength (f_y), MPa	Ultimate tensile strength (f_u), MPa	Modulus of elasticity of reinforcement (E_s), GPa
R6	28.3	421.0	583.0	211.0
R8	50.3	289.0	504.5	207.2
T10	73.8	601.0	644.0	203.0

Table 4 - Ultimate shear, various drift ratios and axial over shear ratios of tested specimens

Specimen	V_{exp}, kN	v_{exp}/f_c'	$v_{Eq\ (1)}/f_c'$	p/v	$DR_{ult\ exp}$, %	$DR_{Eq\ (5)}$, %	$DR_{onset\ collapse}$, %	$DR_{after\ collapse}$, %	$DR_{Eq\ (7)}$, %
C30-N-ALR01	252.5	0.169	0.184	0.87	1.11	1.13	Not detected	Not detected	1.28
C30-N-ALR02	245.0	0.181	0.201	1.55	1.03	0.92	1.11	1.17	0.94
C30-N-ALR03	249.3	0.176	0.193	2.73	0.63	0.62	0.58	0.99	0.63
C30-N-ALR04	250.9	0.175	0.191	3.11	0.47	0.55	0.47	0.49	0.56

Note: V_{exp} is the shear strength of the wall obtained from experiment, v_{exp}/f_c' is the shear stress from experiment (with effective depth of 0.8 wall length) normalised with concrete cylinder strength, $v_{Eq.\ (1)}/f_c$' is the shear stress from Eq. (1) (with effective depth of 0.8 wall length) normalised with concrete cylinder strength, p/v is the ratio of vertical stress to shear stress from experiment, $DR_{ult.\ exp}$ is the drift ratio at shear failure from experiment taken at 20% degradation of peak shear, $DR_{Eq.\ (5)}$ is the drift ratio at shear failure estimated by using Eq. (5), $DR_{onset\ collapse}$ and $DR_{after\ collapse}$ are the drift ratios recorded from experiment at onset of failure and failure after collapse respectively, and $DR_{Eq.\ (7)}$ is the drift ratio at collapse estimated by using Eq. (7).

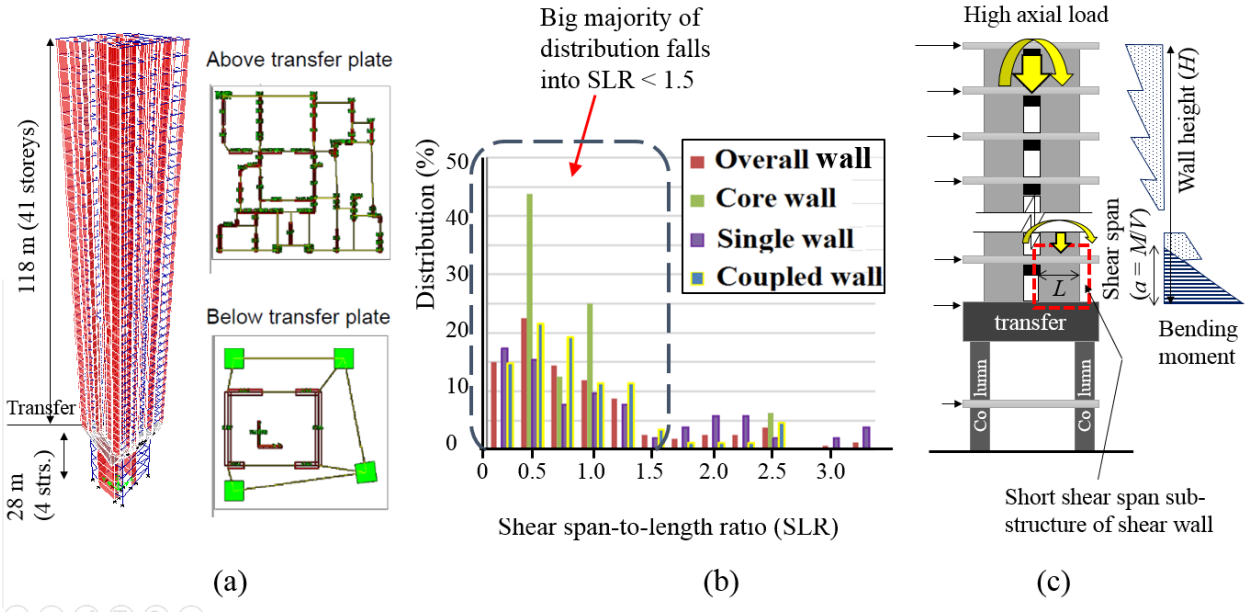

Fig. 1 – (a) 45-storey tall RC building with transfer plate (b) Histogram of shear span-to-length ratio of 45-storey building (c) Definition of short shear span RC walls

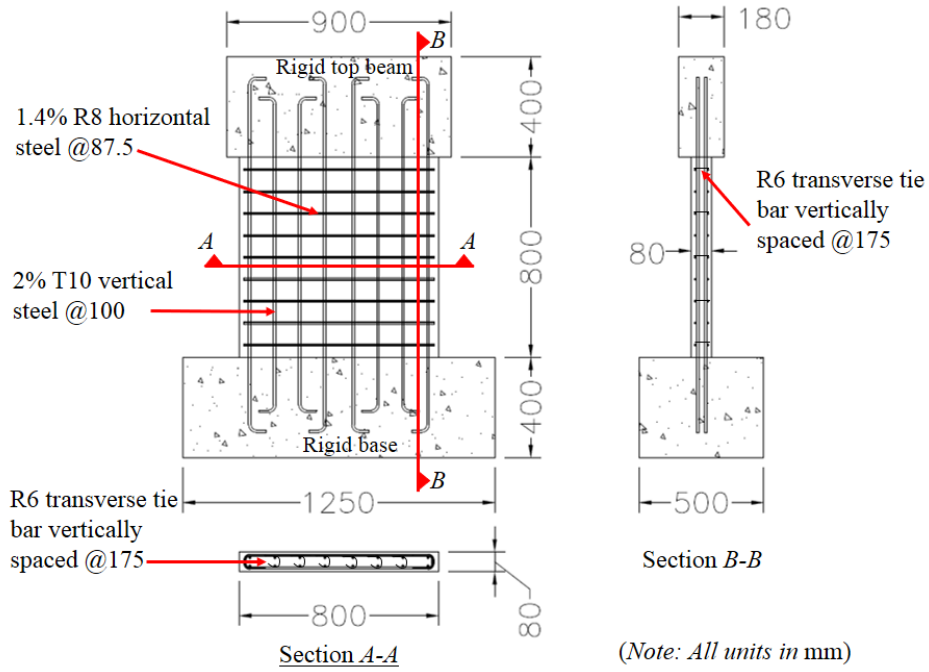

Fig. 2 – Dimensions and reinforcement arrangements of RC walls with short shear span

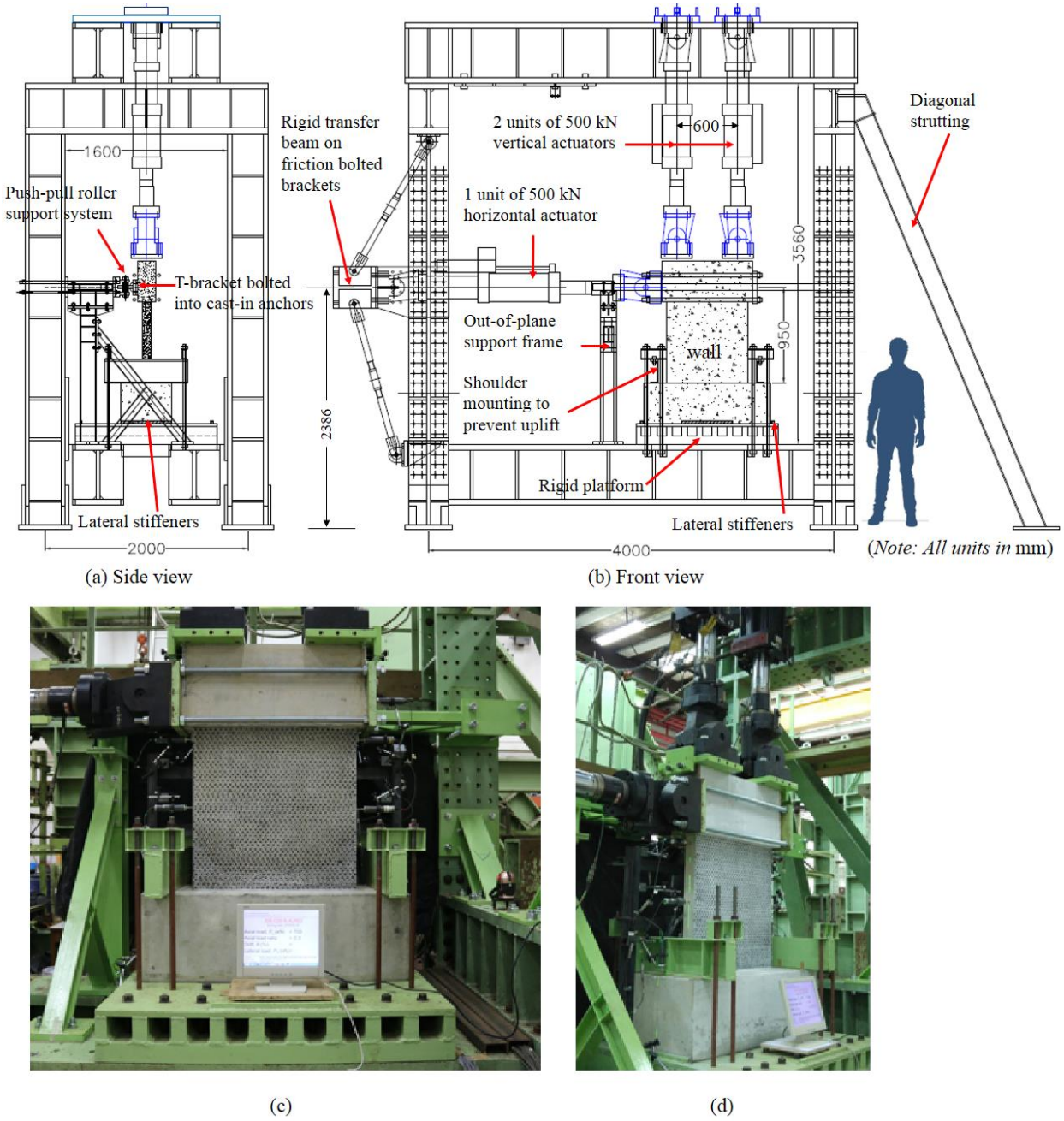

Fig. 3 – (a) Side view drawing (b) Front view drawing (c) Front view of specimen fitted into testing rig (d) Oblique view of specimen fitted into the testing rig

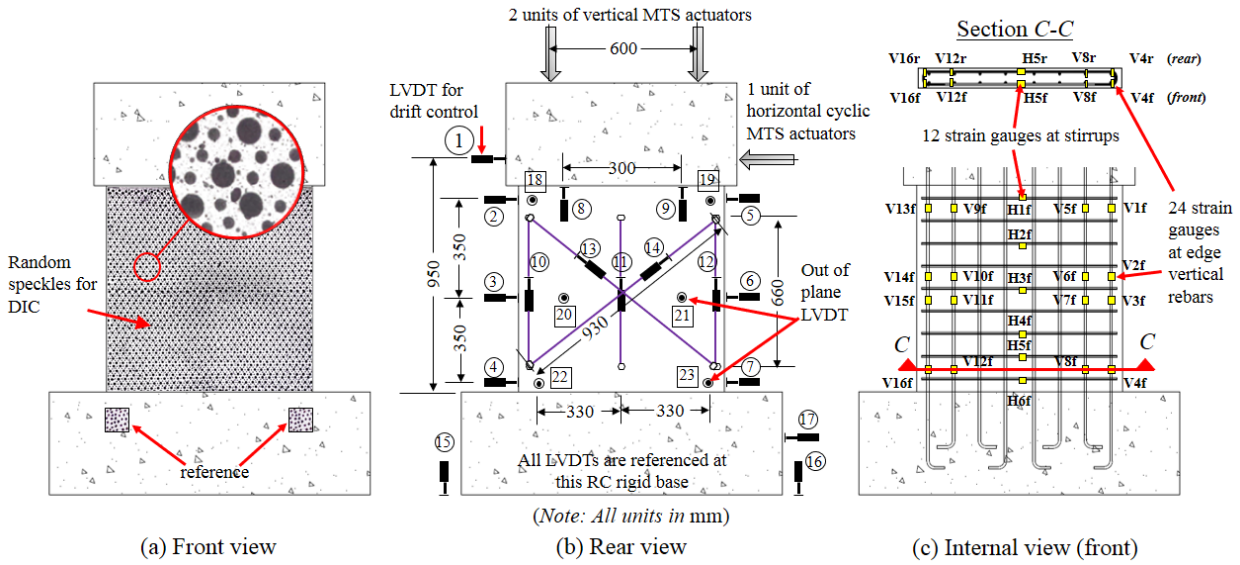

(a) Front view (b) Rear view (c) Internal view (front)

Fig. 4 – Instrumentation (a) Front view with DIC speckles (b) Rear view with LVDTs (c) Inside with strain gauges

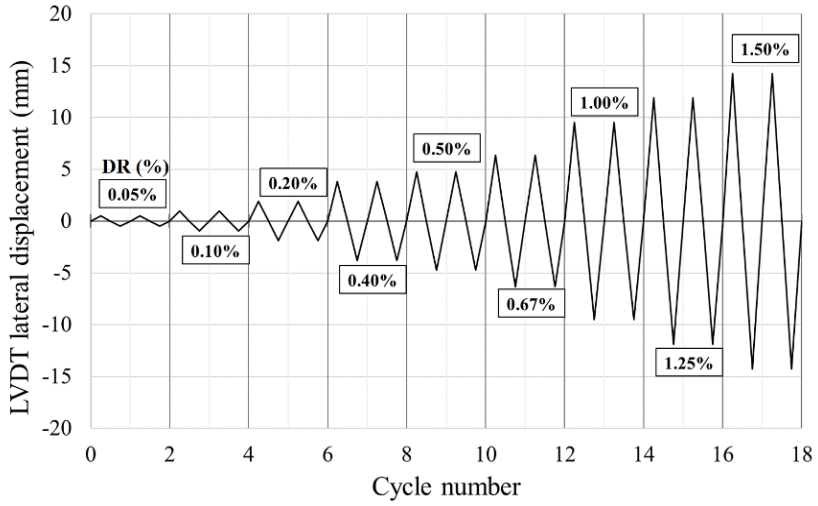

Fig. 5 – Loading protocol

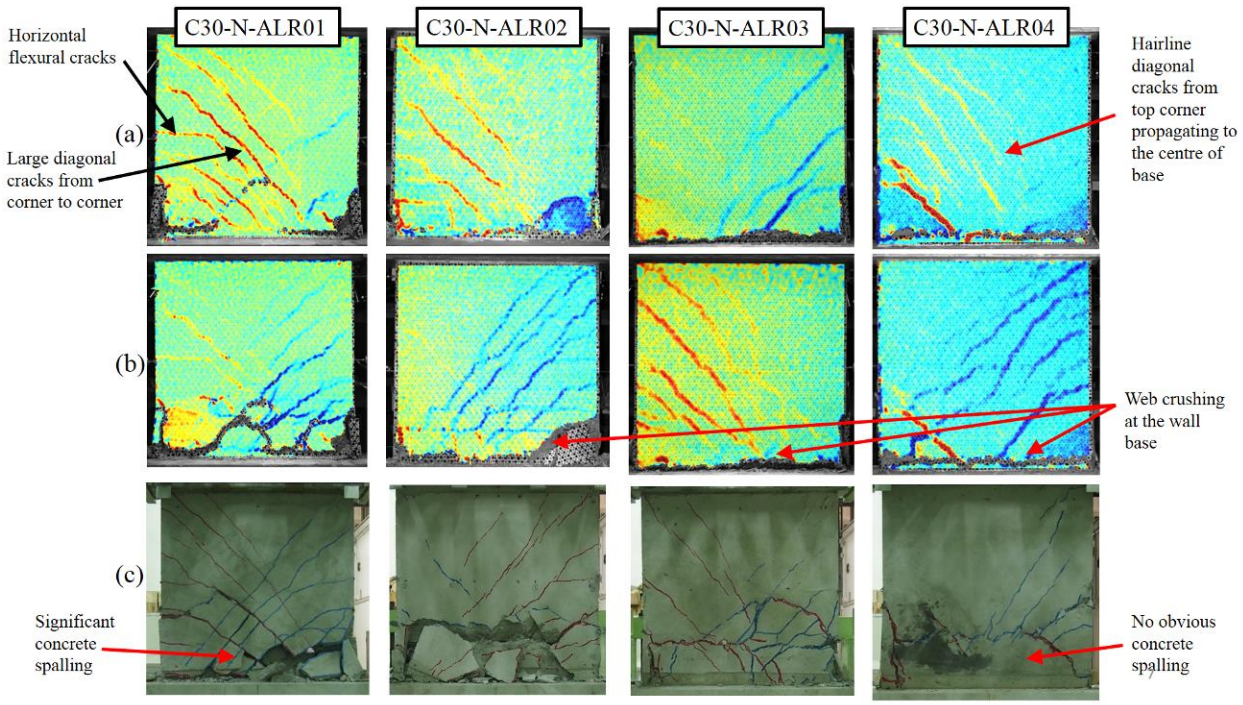

Fig. 6 – Observed failure of walls (a) Front view of cracks by using DIC (b) Front view of cracks drifting at opposite direction by using DIC (c) Rear view of manually drawn cracks

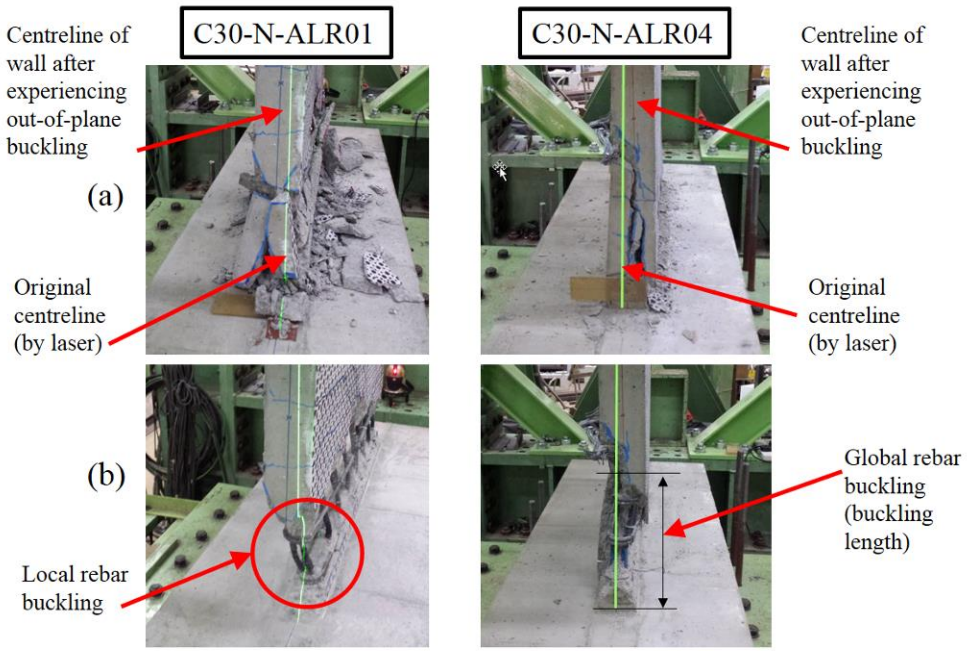

Fig. 7 – Out-of-plane deformation (a) before removal of concrete (b) after removal of concrete

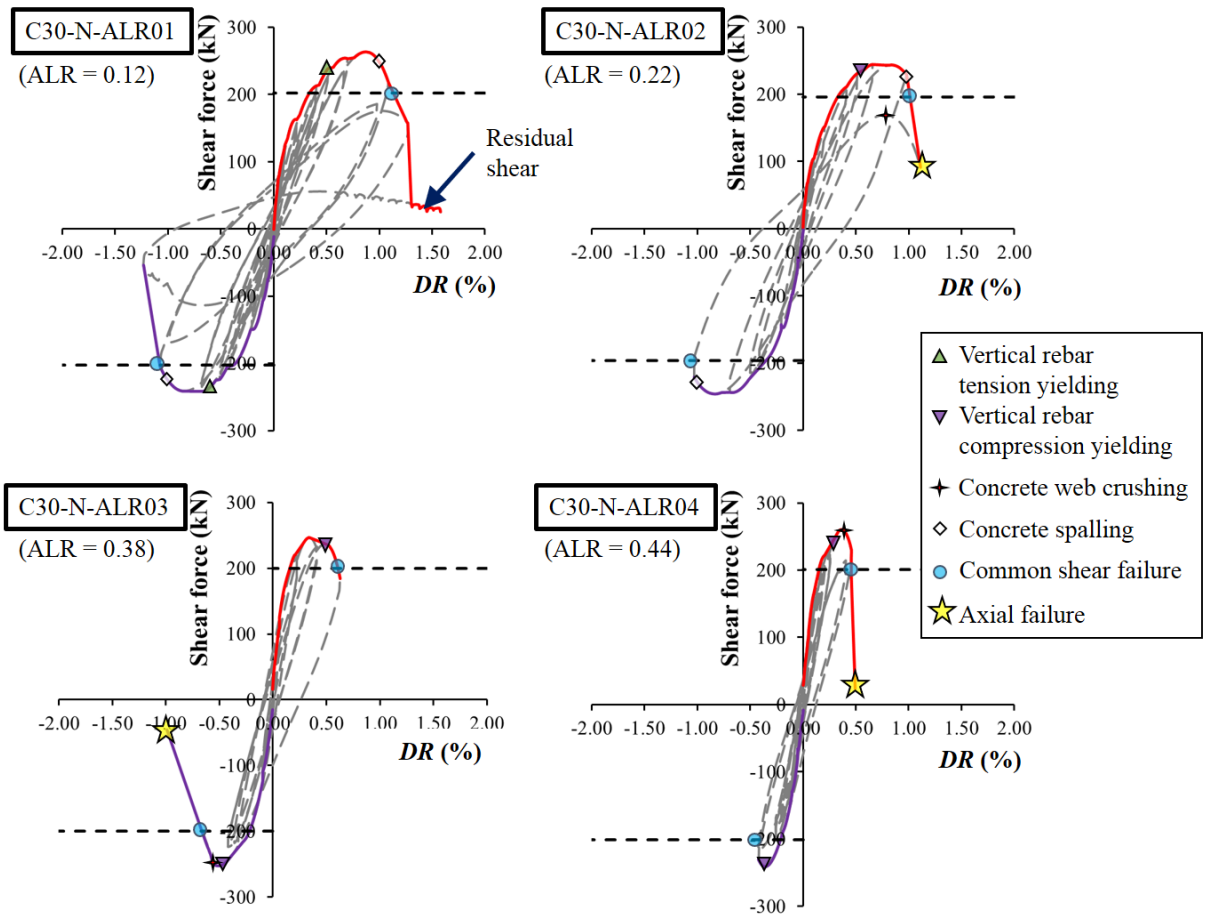

Fig. 8 – Load-displacement hysteresis curve

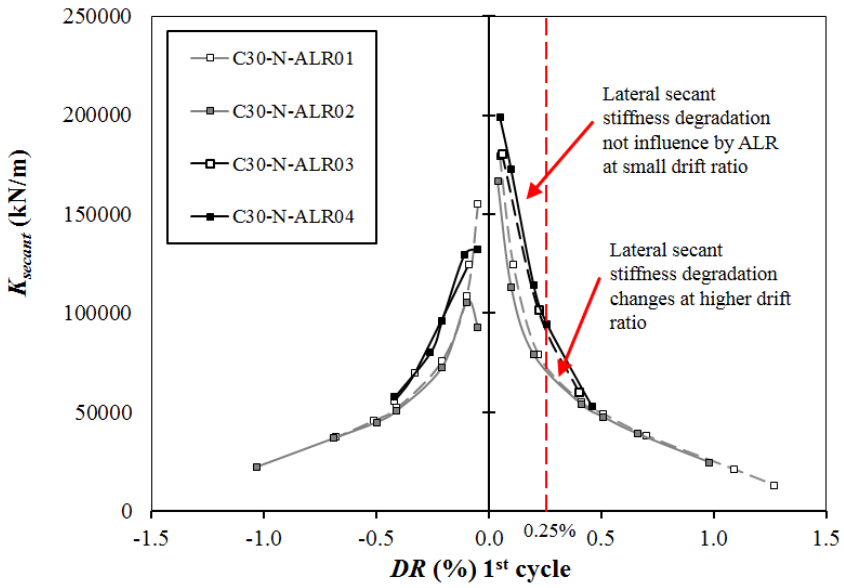

Fig. 9 – Degradation of lateral secant stiffness

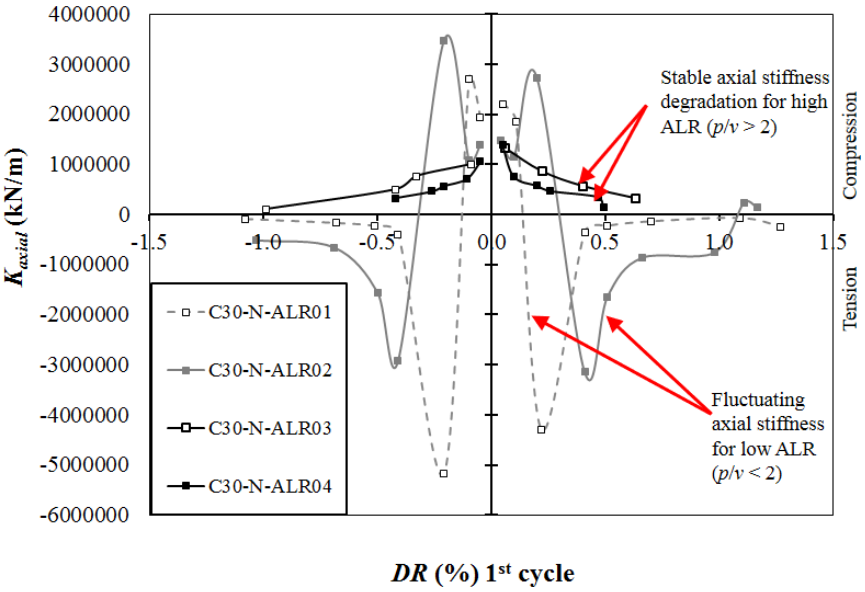

Fig. 10 – Degradation of axial stiffness

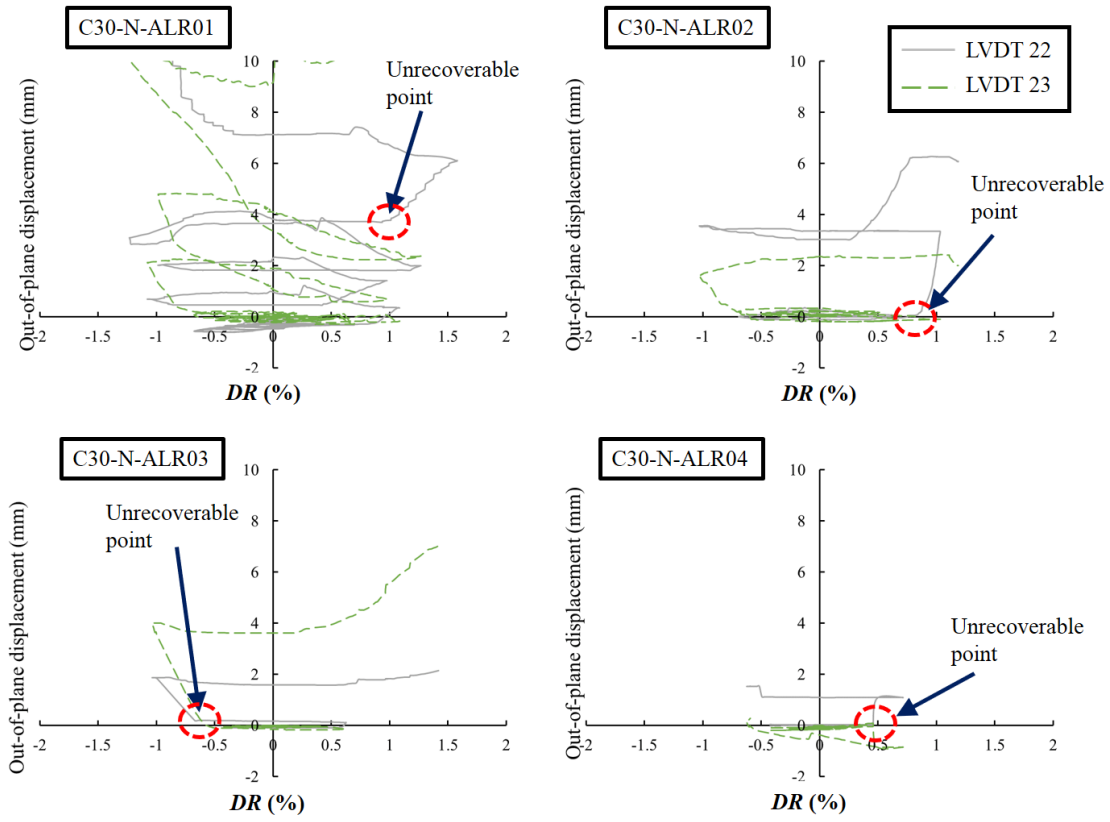

Fig. 11 – Out-of-plane deformation due to in-plane loading

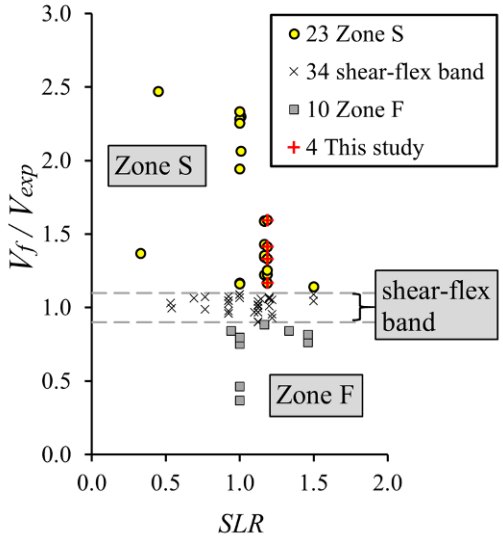

Fig. 12 – Filtered database of rectangular squat RC walls categorised into Zones S and F

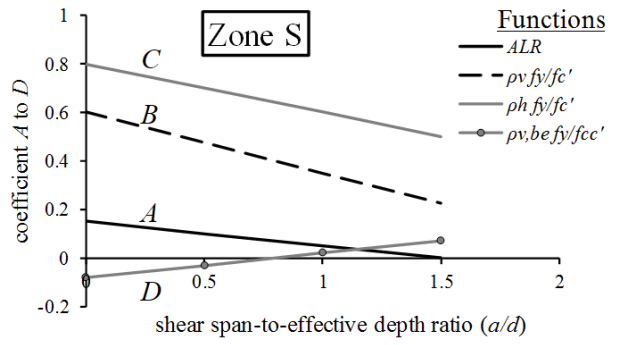

Fig. 13 – Linear functions of proposed shear capacity model for Zone S

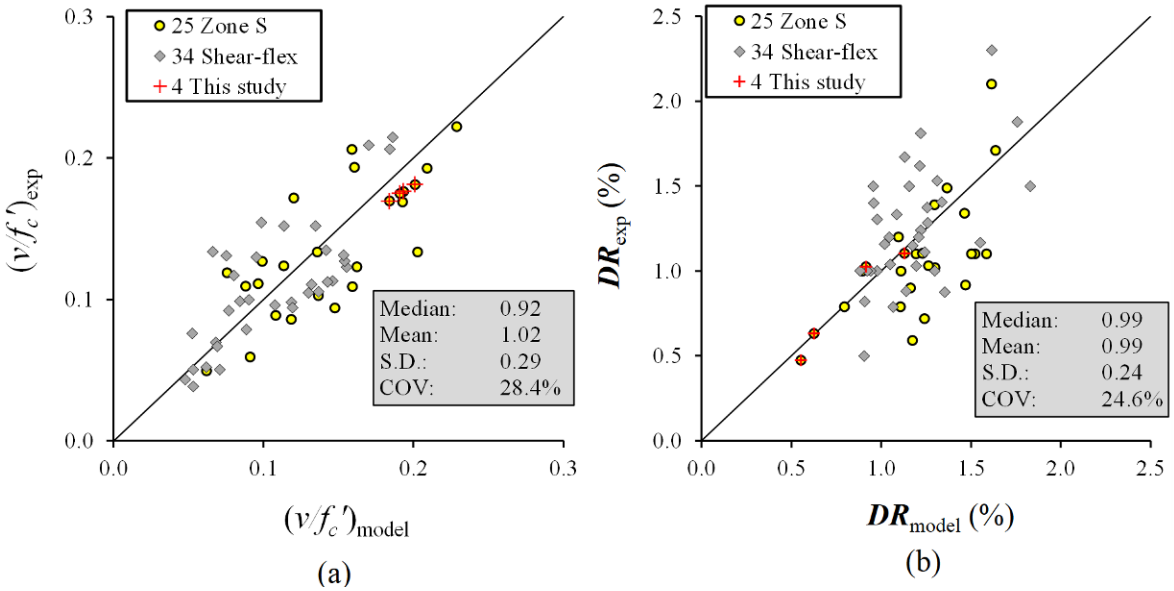

Fig. 14 – Corroboration of experimental results with (a) proposed ultimate shear capacity model for Zone S (b) proposed ultimate drift ratio model for Zone S

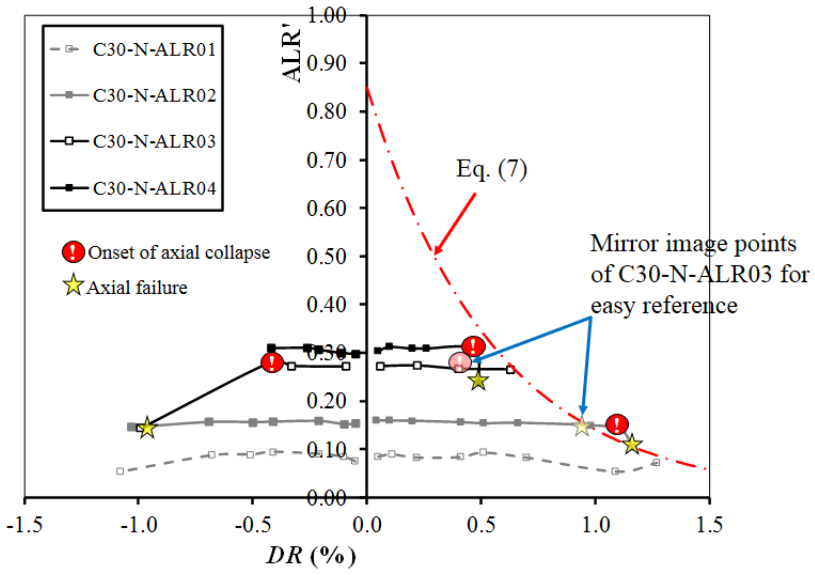

Fig. 15 – Limit of drift due to collapse under axial load for wall with short shear span

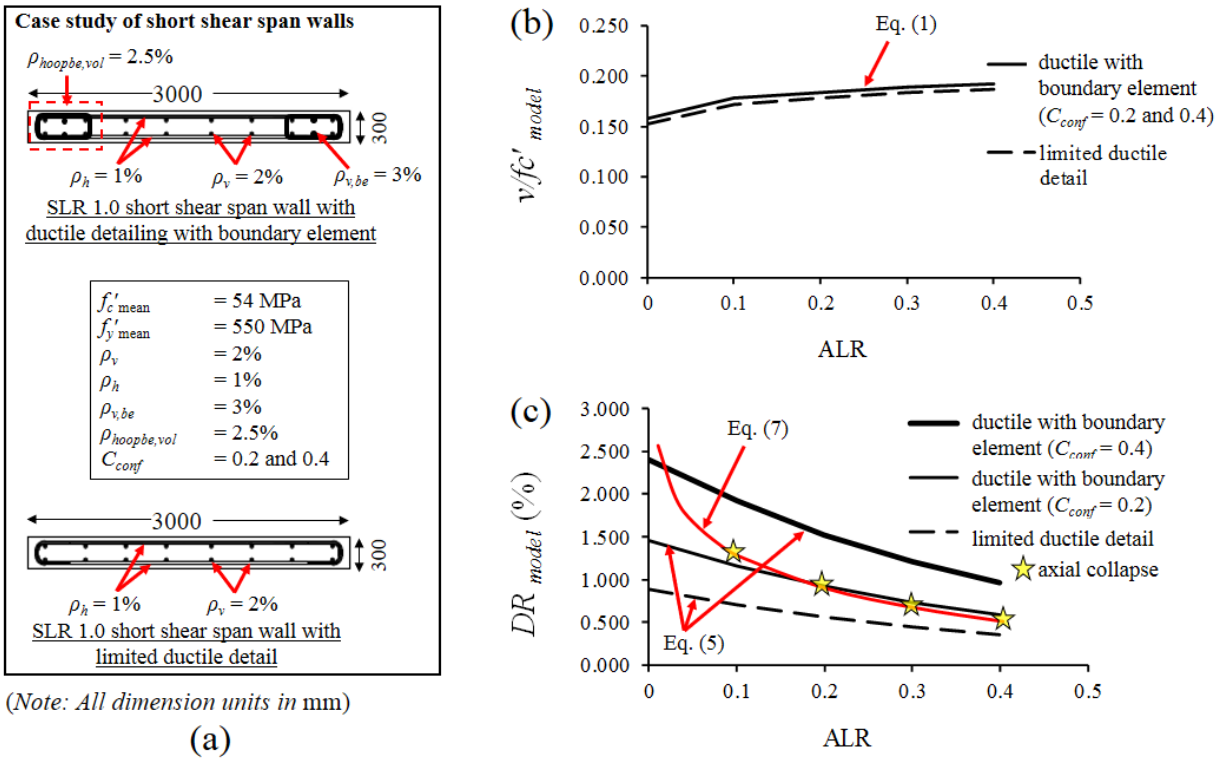

Fig. 16 – Case study - effects of ALR on wall with short shear span (a) properties of walls, (b) variation in shear capacity with ALR, (c) variation in drift ratio capacity with ALR

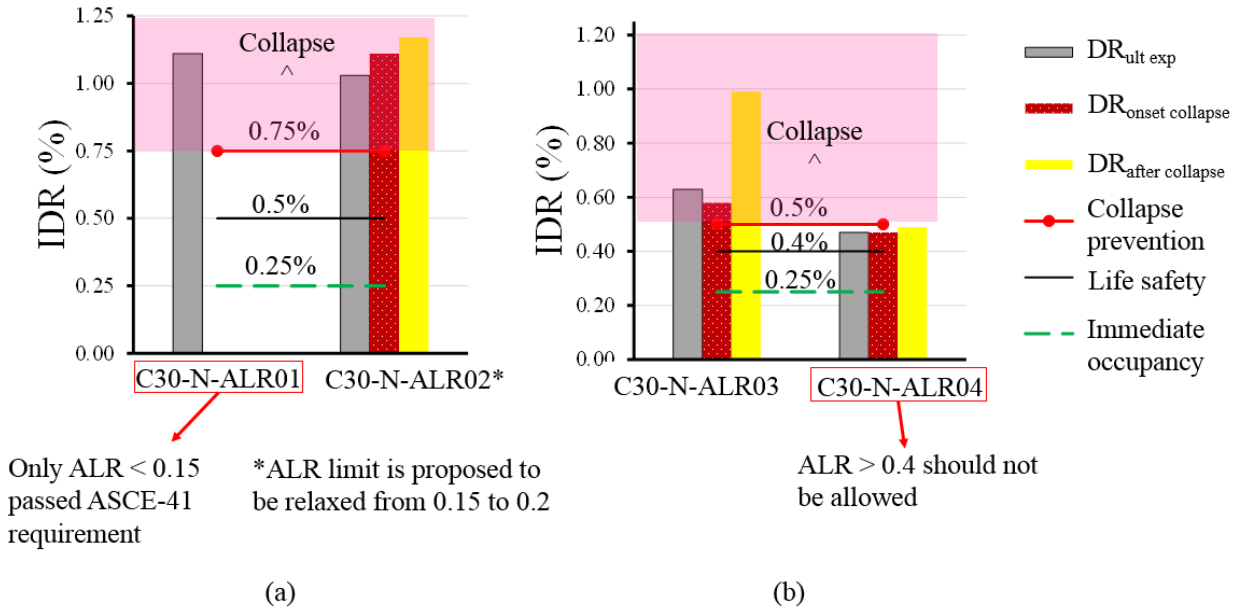

Fig. 17 – Proposal of the inter-storey drift that corresponds to various performance levels of wall specimens with reference to ASCE-41 [26] (a) walls with ALR < 0.2 (b) walls with 0.2 ≤ ALR ≤ 0.4